Letter

Multiple strong topological gaps and hexagonal warping in Bi_4Te_3

Thais Chagas,[1] Omar A. Ashour,[2] Guilherme A. S. Ribeiro,[1] Wendell S. Silva,[3] Zhenglu Li,[2] Steven G. Louie,[2,*] Rogério Magalhães-Paniago,[1,†] and Yves Petroff[3,‡]

[1]*Department of Physics, Federal University of Minas Gerais, Avenida Presidente Antônio Carlos 6627, 31270-901, Belo Horizonte, Brazil*

[2]*Department of Physics, University of California, Berkeley, California 94720, USA and Materials Sciences Division, Lawrence Berkeley National Laboratory, Berkeley, California 94720, USA*

[3]*Brazilian Synchrotron Light Laboratory, Center for Research in Energy and Materials, R. Giuseppe Máximo Scolfaro 10000, 13083-970, Campinas, Brazil*

(Received 8 July 2021; revised 16 November 2021; accepted 31 January 2022; published 17 February 2022)

The electronic topology of Bi_4Te_3, composed of alternating Bi_2 and Bi_2Te_3 layers, is investigated by density functional theory and angle-resolved photoemission spectroscopy. We find, remarkably, that there are three adjacent strong topological gaps with associated protected surface states within a 2-eV range of the Fermi level. The existence of three consecutive Dirac cones in k space gives promise for alternative phenomena and applications, e.g., production of single photons with different energies (in the infrared and visible ranges) for multichannel transport of quantum information as well as multiple degrees of freedom in electron pumping for lasers. Additionally, a surface-state Fermi surface with strong hexagonal warping is observed.

DOI: 10.1103/PhysRevB.105.L081409

I. INTRODUCTION

Topological insulators are known for their protected topological surface states (TSSs), which in three dimensions (3D) commonly manifest as Dirac cones in the fundamental band gap at time-reversal invariant momentum (TRIM) points in the two-dimensional (2D) Brillouin zone (BZ). However, it is rare to find a system with multiple strong topological gaps near the Fermi level [1–3].

The topology of a gap in the bulk electronic structure of 3D topological insulators is characterized by a set of four $\mathbb{Z}_2$ topological invariants, each taking a value of 0 or 1, which dictates the existence of its surface states via bulk-boundary correspondence [4,5]. If the first of these invariants (known as the global invariant) takes on the value of 1, the gap/system is called a strong topological gap/insulator. In this case, there exists a Dirac cone in the corresponding gap of its surface band structure [4]. We show that Bi_4Te_3 is such a remarkable material that has three strong topological gaps, with each gap hosting a surface-state Dirac cone.

Angle-resolved photoemission spectroscopy is a primary tool involved in many seminal discoveries of topological insulators [6]. Bi_2Te_3 [7] and Bi_2Se_3 [8] were among the many topological insulators discovered over the past decade. A Dirac cone of topological surface states exist at the BZ center for both systems: Bi_2Te_3 has a well-studied snowflake-shaped Fermi surface for the TSS [7], while Bi_2Se_3 has a more isotropic Fermi surface [8]. On the other hand, Bi_2 is a topological crystalline insulator whose surface states are protected by spatial and inversion symmetries [9].

Upon alternately stacking Bi_2 bilayers and Bi_2Te_3 or Bi_2Se_3 quintuple layers along the (111) direction, crystals Bi_4Te_3 or Bi_4Se_3 are formed, respectively [10–13]. These two materials are semimetallic. Bi_4Se_3 has been identified as another topological system [11,12] with a snowflake-shaped TSS Fermi surface, more warped than that of Bi_2Te_3 and Bi_2Se_3. One strong topological gap was identified in Bi_4Se_3 [11]. In contrast, Bi_4Te_3 is a very underexplored system, with no studies of its topological properties and only a few studies of its superconducting and vibrational properties [14,15]. Recently, Chagas *et al.* [13] synthesized and investigated the structural and electronic properties of Bi_4Te_3 using x-ray diffraction and scanning tunneling microscopy and spectroscopy.

In this work, we investigate the electronic structure of Bi_4Te_3 through density functional theory (DFT) calculations [16–19] and angle-resolved photoemission spectroscopy (ARPES) experiments. We identify, surprisingly, three strong topological gaps that are adjacent to each other and below the Fermi level of our samples. We investigate both theoretically and experimentally the surface electronic structure of these gaps, identifying three TSS Dirac cones. Additionally, we observe a snowflake-shaped 2D Fermi surface (i.e., constant energy contour of the TSS as a function of wave vector $\boldsymbol{k}_{//}$ parallel to the surface) at the experimentally observed Fermi energy. In contrast to Bi_2Te_3 and Bi_4Se_3, it shows a more elongated structure in the $\bar{\Gamma}$–$\bar{M}$ direction, indicating a strong hexagonal warping effect.

II. RESULTS AND DISCUSSIONS

DFT calculations were carried out using QUANTUM ESPRESSO [16] to analyze the topological properties of Bi_4Te_3 (see Supplemental Material [20]). In Fig. 1(a), the Kohn-Sham DFT band structure of the bulk crystal is plotted. Here, three

*sglouie@berkeley.edu
†rogerio.paniago0@gmail.com
‡yves.petroff@gmail.com

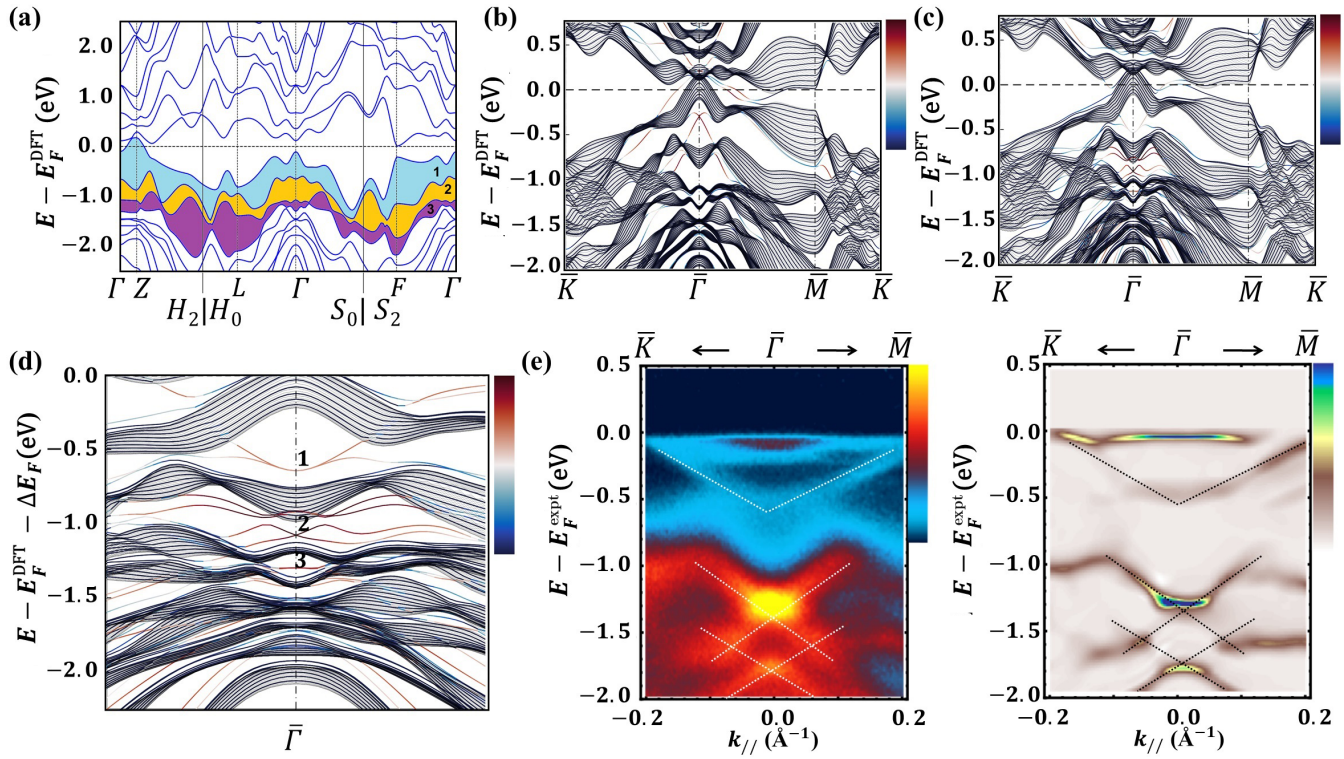

FIG. 1. (a) Band structure of bulk Bi_4Te_3, showing the three strong topological gaps of interest. (b,c) 2D band structure of (b) the Bi_2-terminated slab and (c) the Bi_2Te_3-terminated slab. (d) Close-up view of (c), highlighting the three Dirac cones. For ease of comparison with the experimental results (*n* doped) shown in (e), the theoretical Fermi level E_f^{DFT} is shifted by $\Delta E_f = +0.11$ eV from (c). In (b–d), the thin gray lines (shading) denote the bulk bands projected onto the surface BZ, and the color scale for the slab states (the curves) denotes surface projection of the wave function P_{nk} (see Supplemental Material [20]): deeper red (blue) means closer to the surface (bulk). (e) ARPES measurements (at $h\nu = 21.2$ eV) of the band dispersions of Bi_4Te_3, (left panel) raw data, and (right panel) after treatment using the curvature method [21]. The dashed lines highlight the three sets of Dirac TSS.

band gaps, labeled 1–3 (with different colors), can be identified. The bulk and surface BZs are given in the Supplemental Material [20]. We compute the topological invariants of the three gaps via the parity eigenvalues at the TRIM [4]. The energy gaps, together with their energy ranges (referenced to the Fermi level of a neutral system), at $\bar{\Gamma}$ in the surface BZ as well as their $\mathbb{Z}_2$ topological invariants and classification, are listed in Table I. All three gaps are strong topological ones [4,5], and thus a surface-state Dirac cone is expected at the $\bar{\Gamma}$ point in all three gaps at the surface.

Bi_4Te_3 can have two types of surface terminations, i.e., a Bi_2 or Bi_2Te_3 layer [13]. The theoretical band structures of these two surface terminations, calculated via DFT, are presented in Figs. 1(b) and 1(c), respectively. Figure 1(d) provides a close-up view of the theoretical TSS bands of the Bi_2Te_3-terminated surface found in all three strong topological gaps. For Bi_4Se_3, on the other hand, only one topological gap has been identified [11], and different topological surface states are present for the two terminations, i.e., the Bi- or Se-rich surfaces [11,10].

TABLE I. Energy gap range at $\bar{\Gamma}$ and topological indices of gaps 1–3 [see Fig. 1(a)]. The energy gap range is determined along the $\Gamma - Z$ path in the bulk BZ, which is folded to the $\bar{\Gamma}$ point of the surface BZ that hosts the surface Dirac points. The theoretical Fermi level is set to 0 eV in this table.

Gap	Energy range along $\Gamma - Z$	$\mathbb{Z}_2$ Index	Classification
1	−0.11 to −0.66 eV	(1;000)	Strong
2	−0.88 to −1.07 eV	(1;111)	Strong
3	−1.08 to −1.30 eV	(1;111)	Strong

The Bi_4Te_3 samples investigated experimentally here were synthesized using the Bridgman method as described in [13] (see Supplemental Material [20]). The left panel of Fig. 1(e) presents our system's measured band dispersions (raw data) along the $\bar{K}$–$\bar{\Gamma}$–$\bar{M}$ direction in the first surface BZ. Our measured ARPES data were further analyzed using the curvature method [21], which allows for better visualization of the bands [right panel of Fig. 1(e)]. One observes from the measurement bulk conduction bands around the $\bar{\Gamma}$ point just below the Fermi level, as well as three sets of Dirac TSS ranging from –2.0 eV up to the Fermi level. In particular, the topmost V-shaped band deviates from a linear dispersion along the $\bar{\Gamma}$–$\bar{M}$ direction near the Fermi level. This gives rise to a measured snowflake-shaped TSS Fermi surface with branches pointing along the $\bar{\Gamma}$–$\bar{M}$ direction, as presented in Fig. 2 and further discussed later [22–24]. Strong anisotropic warping effects presented in Bi_4Te_3 significantly reshape the Dirac cone to V-shaped bands in gap 1.

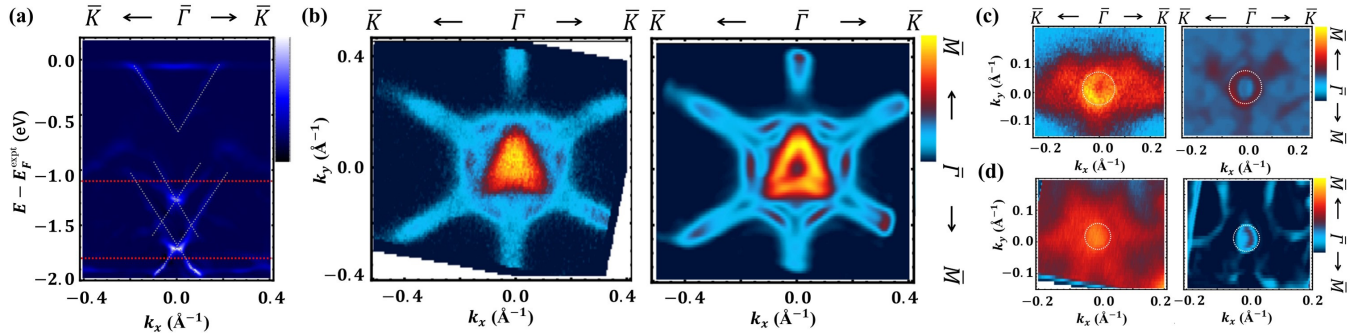

FIG. 2. (a) ARPES measurements of the band dispersions of Bi_4Te_3 along the $\bar{K}$–$\bar{\Gamma}$–$\bar{K}$ direction in the surface BZ after treatment using the curvature method [21]. The white dashed lines highlight the three sets of Dirac TSS, while the red dashed lines mark the positions in which the CECs, shown in (c,d), were measured. (b) The 2D Fermi surface and (c) CEC measured at –1.12 eV and (d) –1.81 eV (left panels present raw data, while the right ones present treated data). ARPES measurements were taken using photon energies of (a) 26, (b) 18, (c) 18, and (d) 18 eV.

The measured Dirac point of the first cone is located at –0.55 eV, in close agreement with the theoretical results of –0.6 eV (the theoretical Fermi level is shifted by +0.11 eV to align with the experimental value of our *n*-doped sample, matching the observed Fermi surface geometry). In addition, the curvature analysis [21] of the ARPES data shows bands with linear dispersion in the second topological gap, which meet at $\bar{\Gamma}$ near –1.30 eV (the corresponding theoretical value is at –1.1 eV). The dashed lines are guides for the eyes. Finally, another set of two linearly dispersing bands in the third topological gap that meet at $\bar{\Gamma}$ near –1.78 eV (theoretical value is at –1.3 eV) is also seen. Thus, the surface states in the topological gaps 1–3, theoretically predicted for this system with Bi_2Te_3 termination, are well identified experimentally. Moreover, the experimental and theoretical energies of the Dirac points are also in good agreement. These results show that there are three strong topological gaps in Bi_4Te_3 and the sample investigated is mostly Bi_2Te_3 terminated. For a comparison of the theoretical and experimental constant energy contours (CECs), see the Supplemental Material [20].

To investigate the different physical characteristics of the multiple Dirac cones, we compute the projection of the states of the three Dirac cones to all angular momentum components for *p* orbitals as a function of distance into the bulk in the presence of spin-orbit coupling (SOC). We observe very distinct wave-function characters for the three Dirac cones, in terms of surface localization and angular momentum components. Such differences in the character of the cones can enable, for example, a precise excitation of each of them using different light polarization (see Supplemental Material [20]).

To experimentally confirm the surface-state nature of the linear bands located around the $\bar{\Gamma}$ point, the surface electronic structure of Bi_4Te_3 was investigated using different photon energies. The data analysis shows no energy dispersion of the states in the topological gaps by changing photon energy, demonstrating that the observed states are indeed surface states (see Supplemental Material [20]).

In Fig. 2(a) the measured band dispersions of the multiple Dirac cones are depicted after treatment for better visualization [21]. In Fig. 2(b) the raw data of the 2D Fermi surface are shown (left panel) as well as after treatment (right panel). The surface-state Fermi surface depicted in Fig. 2(b) shows a snowflake shape for the Dirac cone in gap 1 which, as discussed in the Supplemental Material [20], does not disperse with photon energy variation. The inner band inside this structure is a conduction bulk band that has a threefold symmetry for incident photon energy of 21.2 eV. One also observes that the warped 2D Fermi surface of Bi_4Te_3 has structures resembling branches which extend over to the BZ border along the $\bar{\Gamma}$ –$\bar{M}$ direction, different from what are found in Bi_2Te_3 [7].

In Fig. 2(c) the constant energy contour [data taken at 1.12 eV below the Fermi level—see the red dashed line in Fig. 2(a)] of Dirac cone 2 is shown before and after treatment in the left and right panels, respectively. Here, in contrast to the previous case shown in Fig. 2(b), the CEC presents a circular shape similar to Bi_2Se_3 [25]. Finally, the band dispersion of Dirac cone 3 and its CEC measured at 1.81 eV below the Fermi level are seen in Figs. 2(a) and 2(d), respectively.

Additional ARPES measurements were performed to further investigate the structure observed in the hexagonal CECs that seem to cross the BZ boundary at the Fermi level along the $\bar{\Gamma}$–$\bar{M}$ direction. In particular, the use of higher photon energies allowed us to probe higher-order BZs to better understand the physical phenomena taking place at the edges of the BZ. The 2D Fermi surface in the extended BZ of Bi_4Te_3 is shown in Fig. 3(a) via the ARPES spectra measured using synchrotron radiation with an energy of 103.5 eV. In Fig. 3(b) the TSS in the $\bar{K}$–$\bar{\Gamma}$–$\bar{K}$ direction is presented both before and after the treatment in the upper and bottom panels, respectively. Figure 3(c) depicts the raw (upper panel) and treated (bottom panel) band dispersion of the TSS between the first and second BZs crossing the $\bar{M}$ point, along the $\bar{\Gamma}$–$\bar{M}$–$\bar{\Gamma}$ direction. CECs collected at 0.30 eV below the Fermi level between the boundaries of the first and second BZs (see the white dashed line separating them) and close to the $\bar{M}$ point are shown in Fig. 3(d) for the raw and treated data in the upper and bottom panels, respectively. This figure clearly highlights a Fermi surface structure crossing the first and the second BZ. Due to the experimental resolution of 50 meV, this structure that crosses the $\bar{M}$ point may be at the Fermi level or a few meVs below.

The hexagonal CECs observed in Figs. 2 and 3 are similar to those found for the Bi_2Te_3 TSS Fermi surface [7]. The

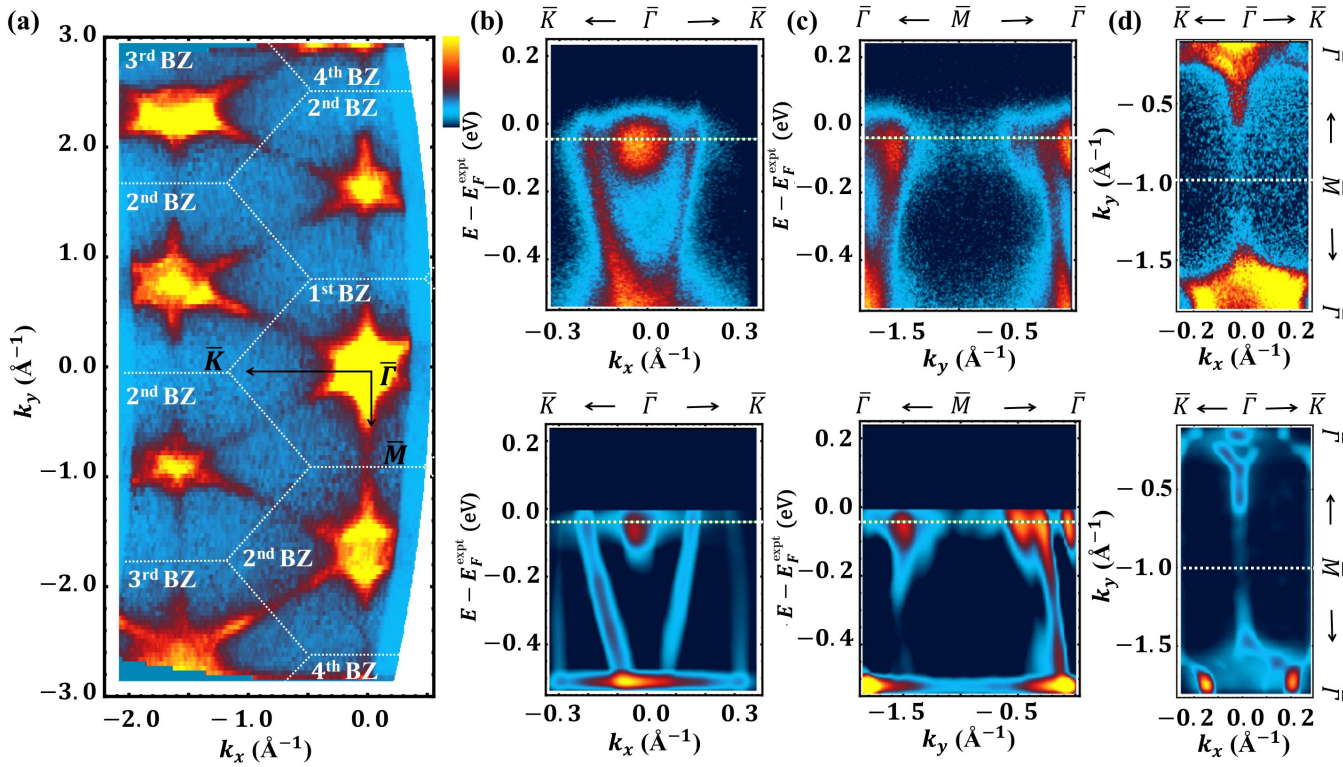

FIG. 3. ARPES spectra of Bi_4Te_3 using synchrotron radiation $h\nu = 103.5$ eV. (a) Extended BZ scheme of a CEC taken at 0.30 eV below the Fermi level, showing elongated structures of the TSS which extend across the BZ edges along $\bar{\Gamma}$–$\bar{M}$. (b) TSS along the $\bar{K}$–$\bar{\Gamma}$–$\bar{K}$ direction. (c) Band dispersion between the first and second surface BZ crossing the $\bar{M}$ point. (d) CECs collected at 0.30 eV below the Fermi level highlighting the states which extend along the $\bar{\Gamma}$–$\bar{M}$ direction. Raw and treated data are depicted in the upper and bottom panels, respectively, of (b–d).

Fermi surface warping effect has been theoretically modeled in Ref. [26], and here we use its variant to quantify the hexagonal warping in our TSS Fermi surface at fixed Fermi energy. We fit the data to the following function:

$$1 = A\sqrt{\kappa^2 + \lambda^2\kappa^6\cos^2(3\theta)}, \tag{1}$$

where A is a measure of the Fermi surface's size, κ is the electron crystalline momentum, λ is a hexagonal warping parameter, and θ is the azimuth angle of $\vec{\kappa}$ with respect to the $\bar{\Gamma} - \bar{K}$ direction. Using this equation, we have investigated the CECs of Bi_4Te_3, by fitting the two parameters A and λ.

In Fig. 4(a), the measured TSS Fermi surface of Bi_4Te_3 is presented. The red line superimposed on the figure is the fit for our system using Eq. (1), with $\lambda = 27.77$ Å^2 and $A = 2.668$ Å. In Fig. 4(b), the theoretical Fermi surface obtained from DFT (at E_f^{expt}) is shown, and the magenta line represents the fit to Eq. (1) with $\lambda = 41.02$ Å^2 and $A = 2.110$ Å. The considerably large values of λ manifest the strongly warped Fermi surface, in contrast to the isotropic case with no warping, i.e., $\lambda = 0$, such as in Bi_2Se_3.

III. CONCLUSION

In conclusion, we have studied the bulk and surface electronic structure of Bi_4Te_3 employing a combination of theoretical and experimental techniques. DFT was used to study the bulk electronic structure of our system, in particular its band topology, as well as its surface properties with Bi_2Te_3 and Bi_2 surface terminations. This revealed the existence of three strong topological gaps near the Fermi level, leading to multiple TSS Dirac cones at the center of the 2D BZ. The electronic properties were investigated experimentally utilizing ARPES measurements that confirmed the presence of these multiple TSSs. A direct comparison between the theoretical and experimental results strongly supports that Bi_4Te_3 has three adjacent strong topological gaps near its Fermi level, and that the Bi_2Te_3-terminated surface is the main surface

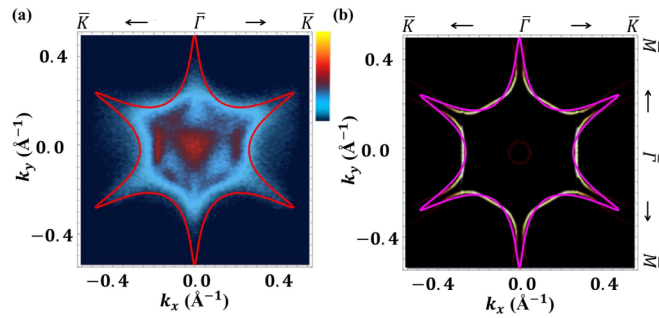

FIG. 4. Fit results with Eq. (1) to the TSS Fermi surface of Bi_4Te_3 with Bi_2Te_3 termination (a) to the experimental data with $h\nu = 21.2$ eV ($\lambda = 27.77$ Å^2 and $A = 2.668$ Å) and (b) to the DFT data (at the experimental E_F; $\lambda = 41.02$ Å^2 and $A = 2.110$ Å).

termination for our cleaved samples. Considering the remarkable existence of three consecutive Dirac cones near E_F, one can foresee a number of unique phenomena and applications. Since the Dirac cones are at the same k point, the production of single photons with different energies (in the infrared and visible ranges) allows for multichannel transport of information and its storage. These states below E_F can also be used as a multibit configuration for quantum information. Finally, highly anisotropic CECs near the Fermi level are observed, with the warping being more significant than in Bi_2Te_3. Our joint experiment-theory study here paves the way for exciting further studies of a clearer and deeper understanding of Bi_4Te_3 and other multiple strong topological gap materials.

ACKNOWLEDGMENTS

The authors acknowledge experimental support by the Brazilian Synchrotron Light Laboratory (LNLS, Brazil). We also acknowledge Elettra Sincrotrone Trieste for providing access to its synchrotron radiation facilities and we thank Ivana Vobornik, Debashis Mondal, and Jun Fujii for assistance in using beamline APE-LE. This study was financed in part by the Coordenação de Aperfeiçoamento de Pessoal de Nível Superior–Brazil (CAPES), Finance Code No. 001 and the Brazilian funding agencies FAPEMIG and CNPq. T.C. acknowledges financial support from CAPES-Print Process No. 88887.474492/2020-00. The theoretical and computational study in this work was supported by the National Science Foundation under Grant No. DMR-1926004. Computational resources were provided by Cori at National Energy Research Scientific Computing Center (NERSC), which is supported by the Office of Science of the U.S. Department of Energy under Contract No. DE-AC02-05CH11231, and by Frontera at TACC, which is supported by the National Science Foundation under Grant No. OAC1818253.

T.C. and O.A.A. contributed equally to this paper. R.M.-P., Y.P., and S.G.L. designed and directed the research. T.C., G.A.S.R., W.S.S., R.M.-P., and Y.P. performed angle-resolved photoemission spectroscopy measurements. O.A.A., Z.L., and S.G.L. performed DFT calculations and theoretical analyses. T.C. and R.M.-P. grew and characterized the samples. All authors contributed to the writing of the paper.

[1] X.-A. Nie, S. Li, M. Yang, Z. Zhu, H.-K. Xu, X. Yang, F. Zheng, D. Guan, S. Wang, Y.-Y. Li, C. Liu, J. Li, P. Zhang, Y. Shi, H. Zheng, and J. Jia, Robust hot electron and multiple topological insulator states in $PtBi_2$, ACS Nano **14**, 2366 (2020).

[2] B. R. Ortiz, S. M. L. Teicher, Y. Hu, J. L. Zuo, P. M. Sarte, E. C. Schueller, A. M. Milinda Abeykoon, M. J. Krogstad, S. Rosenkranz, R. Osborn, R. Seshadri, L. Balents, J. He, and S. D. Wilson, CsV_3Sb_5: A $\mathbb{Z}_2$ Topological Kagome Metal with a Superconducting Ground State, Phys. Rev. Lett. **125**, 247002 (2020).

[3] H. Tan, Y. Liu, Z. Wang, and B. Yan, Charge Density Waves and Electronic Properties of Superconducting Kagome Metals, Phys. Rev. Lett. **127**, 046401 (2021).

[4] L. Fu and C. L. Kane, Topological insulators with inversion symmetry, Phys. Rev. B **76**, 045302 (2007).

[5] L. Fu, C. L. Kane, and E. J. Mele, Topological Insulators in Three Dimensions, Phys. Rev. Lett. **98**, 106803 (2007).

[6] B. Lv, T. Qian, and H. Ding, Angle-resolved photoemission spectroscopy and its application to topological materials, Nat. Rev. Phys. **1**, 609 (2019).

[7] Y. L. Chen, J. G. Analytis, J.-H. Chu, Z. K. Liu, S.-K. Mo, X. L. Qi, H. J. Zhang, D. H. Lu, X. Dai, Z. Fang, S. C. Zhang, I. R. Fisher, Z. Hussain, and Z.-X. Shen, Experimental realization of a three-dimensional topological insulator, Bi_2Te_3, Science **325**, 178 (2009).

[8] Y. Xia, D. Qian, D. Hsieh, L. Wray, A. Pal, H. Lin, A. Bansil, D. Grauer, Y. S. Hor, R. J. Cava, and M. Z. Hasan, Observation of a large-gap topological-insulator class with a single Dirac cone on the surface, Nat. Phys. **5**, 398 (2009).

[9] C.-H. Hsu, X. Zhou, T.-R. Chang, Q. Ma, N. Gedik, A. Bansil, S.-Y. Xu, H. Lin, and L. Fu, Topology on a new facet of bismuth, Proc. Natl. Acad. Sci. USA **116**, 13255 (2019).

[10] T. Valla, H. Ji, L. M. Schoop, A. P. Weber, Z.-H. Pan, J. T. Sadowski, E. Vescovo, A. V. Fedorov, A. N. Caruso, Q. D. Gibson, L. Müchler, C. Felser, and R. J. Cava, Topological semimetal in a Bi-Bi_2Se_3 infinitely adaptive superlattice phase, Phys. Rev. B **86**, 241101(R) (2012).

[11] Q. D. Gibson, L. M. Schoop, A. P. Weber, H. Ji, S. Nadj-Perge, I. K. Drozdov, H. Beidenkopf, J. T. Sadowski, A. Fedorov, A. Yazdani, T. Valla, and R. J. Cava, Termination-dependent topological surface states of the natural superlattice phase Bi_4Se_3, Phys. Rev. B **88**, 081108(R) (2013).

[12] A. P. Weber, Q. D. Gibson, H. Ji, A. N. Caruso, A. V. Fedorov, R. J. Cava, and T. Valla, Gapped Surface States in a Strong-Topological-Insulator Material, Phys. Rev. Lett. **114**, 256401 (2015).

[13] T. Chagas, G. A. S. Ribeiro, P. H. R. Gonçalves, L. Calil, W. S. Silva, A. Malachias, M. S. C. Mazzoni, and R. Magalhães-Paniago, Bi_2:Bi_2Te_3 stacking influence on the surface electronic response of the topological insulator Bi_4Te_3, Electron. Struct. **2**, 015002 (2020).

[14] J. R. Jeffries, A. L. Lima Sharma, P. A. Sharma, C. D. Spataru, S. K. McCall, J. D. Sugar, S. T. Weir, and Y. K. Vohra, Distinct superconducting states in the pressure-induced metallic structures of the nominal semimetal Bi_4Te_3, Phys. Rev. B **84**, 092505 (2011).

[15] H. Xu, Y. Song, W. Pan, Q. Chen, X. Wu, P. Lu, Q. Gong, and S. Wang, Vibrational properties of epitaxial Bi_4Te_3 films as studied by Raman spectroscopy, AIP Adv. **5**, 087103 (2015).

[16] P. Giannozzi, O. Baseggio, P. Bonfà, D. Brunato, R. Car, I. Carnimeo, C. Cavazzoni, S. de Gironcoli, P. Delugas, F. F. Ruffino, A. Ferretti, N. Marzari, I. Timrov, A. Urru, and S. Baroni, QUANTUM ESPRESSO toward the exascale, J. Chem. Phys. **152**, 154105 (2020).

[17] J. P. Perdew, K. Burke, and Y. Wang, Generalized gradient approximation for the exchange-correlation hole of a many-electron system, Phys. Rev. B **54**, 16533 (1996).

[18] N. Marzari, D. Vanderbilt, A. De Vita, and M. C. Payne, Thermal Contraction and Disordering of the Al(110) Surface, Phys. Rev. Lett. **82**, 3296 (1999).

[19] M. L. Cohen, M. Schlüter, J. R. Chelikowsky, and S. G. Louie, Self-consistent pseudopotential method for localized configurations: Molecules, Phys. Rev. B **12**, 5575 (1975).

[20] See Supplemental Material at http://link.aps.org/supplemental/10.1103/PhysRevB.105.L081409 for (i) a methodological description of the DFT calculations, sample growth and characterization, and experimental details of the ARPES measurements; (ii) comparison between the experimental and theoretical 2D Fermi surfaces; (iii) computation of the projection of the states of the three Dirac cones to all angular momentum components for *p* orbitals as a function of distance into the bulk in the presence of spin-orbit coupling; (iv) experimental band dispersions of Bi_4Te_3 for different photon energies and analysis of energy distribution curves (EDCs) to investigate the surface-state nature of the linear bands located around the point in our system.

[21] P. Zhang, P. Richard, T. Qian, Y.-M. Xu, and H. Ding, A precise method for visualizing dispersive features in image plots, Rev. Sci. Instrum. **82**, 043712 (2011).

[22] K. Kuroda, M. Arita, K. Miyamoto, M. Ye, J. Jiang, A. Kimura, E. E. Krasovskii, E. V. Chulkov, H. Iwasawa, T. Okuda, K. Shimada, Y. Ueda, H. Namatame, and M. Taniguchi, Hexagonally Deformed Fermi Surface of the 3D Topological Insulator Bi_2Se_3, Phys. Rev. Lett. **105**, 076802 (2010).

[23] S.-Y. Xu, L. A. Wray, Y. Xia, F. von Rohr, Y. S. Hor, J. H. Dil, F. Meier, B. Slomski, J. Osterwalder, M. Neupane, H. Lin, A. Bansil, A. Fedorov, R. J. Cava, and M. Z. Hasan, Realization of an isolated Dirac node and strongly modulated spin texture in the topological insulator Bi_2Te_3, arXiv:1101.3985v1.

[24] I. I. Klimovskikh, D. Sostina, A. Petukhov, A. G. Rybkin, S. V. Eremeev, E. V. Chulkov, O. E. Tereshchenko, K. A. Kokh, and A. M. Shikin, Spin-resolved band structure of heterojunction Bi-bilayer/3D topological insulator in the quantum dimension regime in annealed $Bi_2Te_{2.4}Se_{0.6}$, Sci. Rep. **7**, 45797 (2017).

[25] M. Nomura, S. Souma, A. Takayama, T. Sato, T. Takahashi, K. Eto, K. Segawa, and Y. Ando, Relationship between Fermi surface warping and out-of-plane spin polarization in topological insulators: A view from spin- and angle-resolved photoemission, Phys. Rev. B **89**, 045134 (2014).

[26] L. Fu, Hexagonal Warping Effects in the Surface States of the Topological Insulator Bi_2Te_3, Phys. Rev. Lett. **103**, 266801 (2009).